# Synthesis of Rare Earth (Oxo)nitridocarbonates by Employment of Supercritical Carbon Dioxide, Single-source Precursor, Solid-State and Ion Exchange Reactions.

Martin Zeuner, Ulrich Baisch, Wolfgang Schnick

Zeitschrift für Anorganische und Allgemeine Chemie

# Synthesis of Rare Earth (Oxo)nitridocarbonates by Employment of Supercritical Carbon Dioxide, Single-source Precursor, Solid-State and Ion Exchange Reactions.



| | |
|---|---|
| Journal: | *Zeitschrift für Anorganische und Allgemeine Chemie* |
| Manuscript ID: | zaac.201000159.R1 |
| Wiley - Manuscript type: | Research Report |
| Date Submitted by the Author: | 19-May-2010 |
| Complete List of Authors: | Zeuner, Martin; LMU Munich, Chemistry<br>Baisch, Ulrich; Newcastle University, School of Chemistry<br>Schnick, Wolfgang; LMU Munich, Chemistry |
| Keywords: | Lanthanides, Solid-state reactions, Luminescence, Molecular precursor, Oxonitridocarbonates |
| | |

# Synthesis of Rare Earth (Oxo)nitridocarbonates by Employment of Supercritical Carbon Dioxide, Single-source Precursor, Solid-State and Ion Exchange Reactions

**Sandro Pagano,[a] Martin Zeuner,[a] Ulrich Baisch[a,b] Wolfgang Schnick[a]***

**Keywords:** Lanthanides; Solid-state reactions; Luminescence; Molecular precursor; Oxonitridocarbonates

**Abstract**

Novel synthetic approaches to rare earth nitrido- and oxonitridocarbonates are described. Dioxy mono-carbodiimides ($Ln_2O_2CN_2$) from the second half of the lanthanide series are accessible by insertion of supercritical $CO_2$ into lanthanide amido compounds (e.g. $[(Cp_2ErNH_2)_2]$), forming single-source precursors. Ammonolysis of amorphous carbamate compounds affords phase pure $Ln_2O_2CN_2$, which are also accessible via the crystalline carbamate compound $[Ln_2\{\mu\text{-}\eta^1\text{:}\eta^2\text{-}OC(O\textit{t}Bu)NH\}Cp_4]$ (Ln = Y, Ho, Er, Yb). Urea complexes and homoleptic cyanates of europium and strontium have been synthesized by solid-state reaction of urea with the respective metals. Subsequent thermal treatment (160 - 240 °C) results in formation of solvent-free homoleptic cyanates. The $Eu^{2+}$-doped compounds $[Sr(OCN)_2(urea)]:Eu^{2+}$ and $Sr(OCN)_2:Eu^{2+}$ as well as the respective pure Eu-compounds exhibit strong broad band emissions due to $4f^65d^1\text{-}4f^7$ transitions in the bluish green region. Furthermore, rare earth dicyanamides $Ln[N(CN)_2]_3{\cdot}2H_2O$ as well as $Ln[N(CN)_2]_3$ with Ln = Eu, Tb, Gd have been prepared by ion exchange in aqueous solution, followed by evaporation of the solvent at room temperature. Condensed nitridocarbonates

such as rare earth tricyanomelaminates $[NH_4]Ln[HC_6N_9]_2[H_2O]_7 \cdot H_2O$ with Ln = La-Nd, Sm-Dy have been obtained through ion exchange reactions. The luminescence properties of the europium and terbium dicyanamides as well as the tricyanomelaminates have been explored in detail.

[a] Dr. S. Pagano, Dr. M. Zeuner, Prof. Dr. W. Schnick
Ludwig-Maximilians-Universität München
Department Chemie
Butenandtstraße 5-13 (D), D-81377 München, Germany
Fax: (+49)89-2180-77440
E-mail: wolfgang.schnick@uni-muenchen.de

[b] New address: Dr. U. Baisch
School of Chemistry, Newcastle University, Newcastle upon Tyne, NE1 7RU, United Kingdom
Fax: +44-(0)191-222-6929
E-mail: ulrich.baisch@ncl.ac.uk

## Introduction

Over the last decades, inorganic rare earth compounds have emerged from chemical oddities to advanced functional materials. Classical application areas of lanthanide complexes as well as solid-state compounds are homogeneous and heterogeneous catalysts,[1-3] magnetic devices[4] and materials for light conversion (phosphors).[5] Oxidic and nitridic rare earth compounds play an important role for the development of new materials.

We have focused on the synthesis of reactive lanthanide nitrido-precursors and new solid-state compounds based solely on the elements Ln/O/C/N. The first well-established compound in this system was characterized by Hashimoto et al. in 1995. The series of lanthanide dioxy mono-carbodiimides ($Ln_2O_2CN_2$, Ln = La - Gd) was originally synthesized by reacting the respective oxides with a stream of $NH_3$ at 950 °C in a graphite crucible.[6,7] $Ln_2O_2CN_2$ are built up from $[Ln_2O_2]^{2+}$ layers interconnected by carbodiimide ($CN_2^{2-}$) ions. Owing to the structural affinity to rare earth oxysulfides, which are of significant interest as phosphors for CRT and X-ray scintillators, doped lanthanide dioxy mono-carbodiimides have been investigated thoroughly.[8-16] However, the synthesis of the heavy rare earth lanthanide dioxy mono-carbodiimides (Ln = Tb - Lu) has not been reported until recently.[13,15,16] Due to

the high thermal stability of binary rare earth oxides, carbides and nitrides specific synthesis routes are inevitable to expand the field of lanthanide (oxo)nitridocarbonates. Metathesis reactions between lanthanide halides and lithium cyanamide studied by Meyer et al.[17] gave access to various rare earth carbodiimide compounds characterized in the last years: $La_2O(CN_2)_2$;[18] $Ln_2(CN_2)_3$ (Ln = Y, La - Lu);[19] $Ce_3(CN_2)_3N$;[20] $LiEu_2(CN_2)I_3$;[21] $EuCN_2$.[22] Compared to the rapidly growing field of carbodiimide chemistry other rare earth (oxo)nitridocarbonates such as cyanates, dicyanamides or carbamates have been rarely mentioned in the literature.[23-26] To avoid formation of the thermodynamically favored binary oxides, carbides and nitrides a varied chemistry of rare earth (oxo)nitridocarbonates is strongly dependent on the development of inventive reaction strategies. Consequently, we have focused on low temperature approaches towards other rare earth (oxo)nitridocarbonates including carbamates, carbodiimides, cyanates, dicyanamides and tricyanomelaminates.

The following research report is structured by the respective synthesis strategy – starting with tailor-made precursors, reactions in supercritical $CO_2$ and ammonolysis to afford nanocrystalline LnN and heavy rare earth $Ln_2O_2CN_2$. Subsequently, the utilization of urea as cyanate donor for the controlled synthesis of $M(OCN)_2$ (M = Sr, Eu) is described. Ion exchange reactions for rare earth dicyanamides and tricyanomelaminates will be discussed at the end of this report.

## Reactive Lanthanide Nitride Materials

Novel synthetic approaches targeting binary or ternary nitrogen-containing compounds are of general interest, especially in solid-state chemistry, in which basic compounds are often obtained in a higher purity by non-classical reaction routes. Binary lanthanide nitrides are rare earth materials of fundamental interest. There are, however, only a few successful synthetic approaches known for the synthesis of such simple compounds with defined composition. Our general interest to target new nitride containing materials with molecular-precursor syntheses,[27,28] led us to utilize organolanthanide molecular precursors for solid-state synthesis of highly activated rare earth nitrido compounds (Scheme 1). On this background molecular precursor compounds with ligands exhibiting an adequate thermal lability for subsequent pyrolysis reactions were targeted.[29]

In the 1960s, Wilkinson[30] and Fischer[30-33] synthesized the first rare earth metallocenes and observed their ability to bind ammonia. During our search for reactive lanthanide nitride

materials we have extensively studied the reaction of $Cp_3Ln$ complexes (**1**, Ln = Sm, Dy, Ho, Er, Yb) with liquid ammonia yielding sublimable ammine complexes (**2**).[34] Other lanthanide metallocenes (Ce, Nd, Eu) also reacted with $NH_3$, but did not show thermal stability. Structural analysis, carried out for the first time for $[Cp_3LnNH_3]$ compounds, showed that the Ln–N distances do not increase linearly from Er to Gd. The Gd complex showed surprisingly long Ln-$NH_3$ bonds, and structural analysis of $[Cp_3SmNH_3]$ remains problematic, because of the difficulties to obtain suitable single crystals. Geometry optimizations and calculations of the Gibbs free energies for the ammine products suggested little difference in behavior. Therefore, intermolecular effects during the crystallization process are considered to be responsible for the stabilization of the $NH_3$ group for **2** with Ln = Sm - Yb. Thermal treatment of these ammine complexes yielded the respective dimeric amido complexes $[Cp_2LnNH_2]_2$ **3** (Ln = Dy, Ho, Er, Yb; Scheme 1). In contrast, **2** with Ln = Sm, Gd sublime before decomposition to the amido complex occurs. X-ray data of amido-cyclopentadienyl-lanthanide(III) complexes were collected for the first time and proved the formation of a dimeric species. DFT calculations performed for the respective monomers showed that decomposition to the amide at higher temperatures changes significantly from $[Cp_3DyNH_3]$ (1.60 kcal·mol$^{-1}$) to $[Cp_3SmNH_3]$ (5.83 kcal·mol$^{-1}$), and confirmed the experimental results.[34]

Further pyrolysis of **2** or **3** with inorganic bases (e.g. $LiNH_2$) resulted in the formation of reactive nanocrystalline lanthanide nitride powders **4** with an estimated particle size of about 40 - 90 nm. LiCp was observed as a by-product and was separated easily by using organic solvents or sublimation in vacuo. Only traces of carbon remained in the product after evacuation and thus, a brownish solid LnN was obtained after pyrolysis. The formation of nitride material LnN was monitored by temperature programmed high-temperature in situ X-ray diffraction experiments, which proved the formation of LnN at temperatures less than 300 °C. Scanning electron microscopy (SEM) indicated the formation of agglomerated bulky material (Figure 1a, b), whereas transmission electron microscopy (TEM) measurements of the crude product revealed particle sizes between 80 and 100 nm (Figure 1c). Electron diffraction (ED) experiments on these particles proved the crystallinity of the product and confirmed the formation of LnN (Figure 1d).[34]

**Precursor Approach to Lanthanide Dioxy Mono-Carbodiimides**

Lanthanide metallocenes were observed to be reasonably stable against thermal treatment under inert gas atmosphere. On the other hand they represent a highly reactive molecular precursor species under $CO_2$ atmosphere at temperatures above 200 °C. During our studies on the reactivity of lanthanide amine and amido complexes towards $CO_2$, a number of O/C/N-containing precursors was discovered.[23] Carbon dioxide was used as a pre-organized C/O source forming labile carbamate intermediates. These compounds turned out to be excellent starting materials for the synthesis of hitherto unknown species in the system Ln/O/C/N. The absorption of $CO_2$ and the resulting amorphous products have been studied by IR spectroscopy, elemental analysis, and temperature programmed in situ mass spectrometry (MS) studies.[16]

Two organometallic pathways towards phase-pure synthesis of the heavy lanthanide dioxy mono-carbodiimides have been elaborated. The first involves insertion of $CO_2$ into the amido complex **3** $[(Cp_2ErNH_2)_2]$ to form the single-source precursor $[(Er_2(O_2CN_2H_4)Cp_4]$ (**5**). To provide a deeper insight into the structural characteristics of the carbamate precursor, the second approach targeted the synthesis of a crystalline carbamato complex (**6**) which has been fully characterized. After ammonolysis, the precursor approach yielded the hitherto unknown dioxy mono-carbodiimides of Y, Er, Ho and Yb (**7**; Scheme 1).[16]

Supercritical $CO_2$ ($sc$$CO_2$) allows reactions to be carried out in "liquid" carbon dioxide under mild reaction conditions. The mild temperature conditions (50 °C, 220 bar) are of special interest for these precursor compounds because the latter can be carboxylated before thermal degradation of the Cp ligands occurs.[35-37] Employment of $sc$$CO_2$ allows the controlled synthesis of Ln/O/C/N containing single-source precursors by absorption and fixation of $CO_2$. Elemental analysis of the carboxylation product obtained in $sc$$CO_2$ at 50 °C indicated an atomic ratio Er/O/C/N/H = 2/2/21/2/24 corresponding to the formula $[Er_2(O_2CN_2H_4)Cp_4]$ (**5**). This result corroborates the insertion of one carbon dioxide molecule per dimeric amido complex forming a carbamate moiety. In contrast, the elemental analysis of the carboxylation product obtained in $sc$$CO_2$ at 150 °C exhibits an atomic ratio of Er/O/C/N/H = 2/10/25/2/24. The resulting formula $[Er_2(O_2CNH_2)_2(CO_2)_3Cp_4]$ corresponds to five $CO_2$ molecules per dimeric complex. This extensive coordination at the metal center results in an oxygen-rich

product which can be transformed into $Er_2O_3$ by pyrolysis. These results demonstrate that the amount of $CO_2$ inserted into the complexes is predominantly dependent on the reaction temperature if the pressure is held constant. Furthermore, the findings highlight the importance of adding at least one equivalent of $CO_2$ per amido complex in order to obtain useful carbamate precursors and to avoid the formation of lanthanide oxides during subsequent pyrolysis reactions. Ammonolysis of **5** at 700 °C under $NH_3$ atmosphere in LiCl/KCl flux yielded highly crystalline and phase-pure dioxy mono-carbodiimide $Er_2O_2CN_2$, whose crystal structure was refined based on XRPD data by the Rietveld method.[16]

The overall yield of $Ln_2O_2CN_2$ obtained in four reaction steps based on $Cp_3Ln$ as starting material (Scheme 1) is > 25 mol %. With this synthetic approach it was possible to synthesize pure lanthanide dioxy mono-carbodiimides starting from $NH_3$ and $CO_2$ and the well-known $Cp_3Ln$ complexes. The oxophilic character of the lanthanides is the driving force for the reaction.

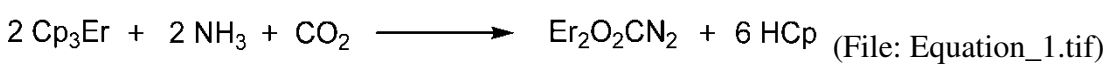

(File: Equation_1.tif)

For the synthesis of a crystalline carbamate complex, *t*-butyl carbamate was considered as an appropriate ligand as it is easily available and exhibits an unprotected amine moiety. As illustrated in Scheme 1, $Cp_3Ln$ (Ln = Y, Ho, Er, Yb, Lu) reacts with one equivalent of *t*-butyl carbamate in toluene to give **6**, as determined by X-ray crystal structure analysis. Comparing the IR data of **6** and **5** add another piece of evidence for formation and characterization of carbamate compounds by insertion of $CO_2$ into lanthanide amido complexes (**3**). Ammonolysis of **6** in analogy to **5** afforded phase-pure and crystalline $Ln_2O_2CN_2$ (Ln = Y, Ho, Er), as proven by elemental analysis and FTIR spectroscopy. The PXRD pattern of $Ln_2O_2CN_2$ (Ln = Y, Ho, Er, Yb) was indexed using similar lattice constants and the same space group as for $Ln_2O_2CN_2$ with Ln = Ce - Gd.[7] The structures were refined in the space group $P\ \bar{3}m1$ by the Rietveld method.[16] Their structure is bulit up from trigonal $[Ln_2O_2]^{2+}$ layers interconnected by carbodiimide ions. The $Ln^{3+}$-ions are coordinated by four oxygen and three nitrogen atoms (Figure 2).

Our studies revealed that the well known $Cp_3Ln$ complexes can be utilized to bind gaseous reactants such as $CO_2$ or even $NH_3$ and thus use them for tailor-made precursor design in the synthesis of solid-state materials to form compounds which are not accessible by standard routes. Nitridic lanthanide materials are of particular interest in materials chemistry of optically active or semiconducting compounds. The reactivity studies of these precursor

compounds towards $CO_2$ reported herein enlarge the potential of amorphous O/C/N-containing solids as future starting materials for the synthesis of new functional materials.

**Urea Route to Homoleptic Cyanates**

Employment of urea to generate alkali metal cyanates starting from alkali salts (oxides, hydroxides, carbonates) is a common synthetic approach. Nevertheless only a few reports[38,39] are known about alkaline earth and lanthanide cyanates and to the best of our knowledge neither systematic investigations nor any structural information has been published for homoleptic cyanates of the latter elements. The decomposition of urea at approximately 130 °C, yielding isocyanic acid and ammonia, can be utilized to oxidize electropositive metals such as Eu or Sr.[40,41] The reaction of three equivalents of urea with Sr or Eu metal in closed ampoules yields $[M(OCN)_2(urea)]$ (M = Sr, Eu), whereas the thermal treatment under vacuum at temperatures of 160 - 240 °C affords evaporation of urea and subsequent formation of solvent-free homoleptic cyanates of Sr and Eu, respectively (see Scheme 2). To avoid oxidation of $Eu^{2+}$ to $Eu^{3+}$ all manipulations were conducted under inert gas atmosphere. For all compounds a phase-pure synthesis was developed and the compounds were fully characterized by means of spectroscopic, magnetic, thermal and crystallographic methods. According to single-crystal X-ray diffraction the isotypic complexes $[M(OCN)_2(urea)]$ (M = Eu, Sr) exhibit a layer-like arrangement of urea and $OCN^-$. The structure is built up from $Eu^{2+}$ centered chains of face-sharing square antiprisms (Figure 3). These chains are connected by cyanate ions to form layers parallel to (100). The $C(NH_2)_2$-backbones of urea are filling the space between the layers and exhibit H-bonding to adjacent cyanato anions. The distance between the adjacent $Eu^{2+}$ atoms (Eu1-Eu1: 3.8969(8) Å) is slightly shorter than the sum of their van-der-Waals radii. No magnetic interactions between the Eu atoms have been detected in the temperature range between 1.8 and 300 K by magnetic measurements. The thermal behavior of $[M(OCN)_2(urea)]$ was investigated by TG/DTA measurements and high-temperature in situ X-ray diffractometry (HT-PXRD). The TG/DTA measurements indicate the onset of the decomposition at 160 °C accompanied by an X-ray amorphous state above 150 °C. In accordance with HT-PXRD the crystalline, homoleptic cyanates of Sr and Eu $M(OCN)_2$ are formed above 200 °C and they are stable up to 500 °C. Further heating to 700 °C results in the formation of $\beta$-$SrCN_2$[42] for $[Sr(OCN)_2(urea)]$ and $Eu_2O_2CN_2$ for $[Eu(OCN)_2(urea)]$;[7] for the latter unknown phases are also observed in the PXRD of the residue. In contrast to the respective thiocyanates of Eu and Sr, cyanates are more temperature sensitive and decompose without melting.[43] The PXRD pattern of $M(OCN)_2$ was indexed

using a similar unit cell setting as that of $Sr(N_3)_2$. Subsequently, starting from the structural model of $Sr(N_3)_2$[44] the crystal structures of $Sr(OCN)_2$ and $Eu(OCN)_2$ were refined in space group *Fddd* by the Rietveld method.[40] The structure consists of one metal site coordinated by 8 cyanate molecules forming square antiprisms. Consequently, each cyanate ion is coordinated to four metal centers (Figure 4). The polyhedra are connected to each other by four common edges. The face-sharing of $Eu^{2+}$ polyhedra in $[M(OCN)_2(urea)]$ is converted into exclusive corner-sharing in $M(OCN)_2$.

Both compounds $[Eu(OCN)_2(urea)]$ and $Eu(OCN)_2$ show strong green to blue emission at low temperatures when irradiated with a UV lamp. However, luminescence is fully quenched at room temperature. A similar behavior has been observed for $M(SCN)_2:Eu^{2+}$ (M = Ca, Sr, Ba).[45] To investigate the luminescence properties of the cyanate compounds in detail we prepared the Eu compounds as well as the Eu-doped Sr compounds $[Sr(OCN)_2(urea)]:Eu^{2+}$ and $Sr(OCN)_2:Eu^{2+}$ (doping rate 0.5 % $Eu^{2+}$). Excitation and emission spectra at different temperatures from 10 K to RT have been collected. The luminescence properties of these compounds and $Sr(SCN)_2:Eu^{2+}$ are summarized in Table 1. Comparison of the luminescent properties of $Sr(OCN)_2:Eu^{2+}$ to those of $Sr(SCN)_2:Eu^{2+}$ is advantageous due to the similarity of the cation coordination polyhedra.[45] The emission curves of all spectra appear nearly in Gaussian shape. This is in accordance with the structural analysis where only one $Eu^{2+}$ site has been located. The excitation spectra represent broad bands without any fine structure. The assignment of the maxima of the lowest excited $5d^14f^7(^7F_0)$ states, which is necessary for the determination of the Stokes shift, is rather difficult because of these broad bands. For all compounds no luminescence spectra could be detected at temperatures above 170 K ($T_{quench}$). The temperature at which the intensity of signal is half of that at 10 K is between 35 and 65 K ($T_{1/2}$). The emission bands for the urea adducts are located in the green region at 513 nm for $[Eu(OCN)_2(urea)]$ and at 501 nm for $[Sr(OCN)_2(urea)]:Eu^{2+}$, whereas signals for homoleptic cyanates are shifted to remarkably higher energies (Table 1); the emission maxima are located at 475 nm for $Eu(OCN)_2$ and 457 nm for $Sr(OCN)_2:Eu^{2+}$. Additionally, the Stokes shift for the homoleptic cyanates is much smaller. This can be explained by the fact that the structure of the homoleptic cyanates is much more rigid and prevents a large increase of the $Eu^{2+}$ ion distance in the excited states. The emission maxima of the urea adducts are similar to $Sr(SCN)_2:Eu^{2+}$ in the green region, whereas the homoleptic cyanates exhibit a strong blue shift. This can be explained by the larger covalency of the host lattice caused by the urea ligand. It shifts the center of gravity of the excited $5d^14f^6$ states to lower energy (nephelauxetic effect). The red shift of the $Eu^{2+}$ emission of homoleptic thiocyanates versus

cyanates can be expected because of the formal replacement of oxygen by sulfur and thus, the more covalent environment around $Eu^{2+}$ in thiocyanates. Compared to the emission maxima of nitrides ($Ba_2Si_5N_8$:$Eu^{2+}$: 590 nm)[46] and simple oxides (SrO:$Eu^{2+}$: 625 nm)[47] signals of the cyanate compounds are significantly shifted towards higher energy.

**Luminescent Rare Earth Dicyanamides**

Investigating the luminescence properties of rare earth dicyanamides is of particular interest as the dicyanamide ion can be regarded as a hybrid between an inorganic ion and a C/N-ligand. However, in the field of lanthanide dicyanamides, most of the solids reported until now are metal-organic dicyanamide complexes such as $[Ln[N(CN)_2]_3(2,2'\text{-bipy})_2(H_2O)]$ with Ln = La, Sm, Gd.[48] We have been able to synthesize hydrated $Ln[N(CN)_2]_3 \cdot 2\,H_2O$ (Ln = Eu, Gd, Tb)[49,50] by ion exchange reactions in aqueous solutions. Evaporation of $H_2O$ at elevated temperatures was followed by the formation of the non-hydrated $Ln[N(CN)_2]_3$ (Ln = La, Ce, Pr, Nd, Sm, Eu, Gd, Tb)[24,49] species. The crystal structures of hydrated $Ln[N(CN)_2]_3 \cdot 2\,H_2O$ have been determined using single-crystal X-ray diffractometry. The hydrated compounds are isostructural and are built up from irregular quadratic antiprismatic $LnN_6O_2$ polyhedra connected to each other by three crystallographically independent dicyanamide ($[N(CN)_2]_3^-$) ions. There are two water molecules completing the coordination sphere of the lanthanide ion (Figure 5). The arrangement of six dicyanamide groups around the lanthanide ion causes a two-dimensional sheet arrangement (Figure 6). The metal ions in two adjacent sheets are approximately 8 Å apart from each other. These layers interact through π-π stacking as well as through hydrogen bonding. The thermal stability of $Ln[N(CN)_2]_3 \cdot 2H_2O$ (Ln = Tb, Eu) has been studied using thermogravimetric and/or differential thermal analysis (TG/DTA). The dehydration of the compound occurs at 150 °C, leading to the formation of anhydrous $Ln[N(CN)_2]_3$, and the rearrangement of dicyanamide groups. The coordination number rises from 8 to 9 because the dicyanamide ion is undergoing two different Ln-N coordination modes: i) $Ln^{\cdots}N\text{-}(CN)_2$ and ii) $Ln^{\cdots}NC\text{-}N\text{-}CN$ (Figure 7). The non-hydrated species are isostructural and have been structurally characterized from powder samples.[24,49]

Figure 8 shows the room-temperature excitation and emission spectra of hydrated $Eu[N(CN)_2]_3 \cdot 2\,H_2O$ and non-hydrated $Eu[N(CN)_2]_3$. The emission spectrum of $Eu[N(CN)_2]_3 \cdot 2\,H_2O$, recorded at $\lambda_{exc} = 365$ nm, shows red luminescence. The typical $Eu^{3+}$

intra-$4f^6$ emission lines were observed, which can be assigned to transitions between the first excited state ($^5D_0$) and the ground multiplets ($^7F_{0\text{-}4}$). The excitation spectrum, monitored at $\lambda_{em}$ = 612 nm is the most intense emission line of $Eu^{3+}$. It exhibits a large broad band between 260 and 420 nm, with a maximum at around 335 nm, superimposed with sharp peaks centered at wavelengths extending from 390 to 550 nm. The sharp peaks can be attributed to inner 4f shell $^7F_0$-$^5L_6$ (395 nm), $^7F_0$-$^5D_3$ (417 nm), $^7F_0$-$^5D_2$ (465 nm), $^7F_0$-$^5D_1$ (525 nm), and $^7F_1$-$^5D_1$ (538 nm) transitions of $Eu^{3+}$.[51] The full width at half-maximum (8000 $cm^{-1}$) of the broad Eu-N charge-transfer band is comparable with that of the Eu-O charge-transfer band in oxide lattices. However, the position of the Eu-N charge-transfer band is significantly shifted to lower energies compared to that of the oxo compounds (nephalauxetic effect). The excitation spectrum of the non-hydrated $Eu[N(CN)_2]_3$ shows features similar to those of the spectrum of the hydrated compound except for a slight shift (~10 nm) of the excitation maximum towards a longer wavelength (348 nm), indicating that excitation mechanisms are essentially the same for both the hydrated and non-hydrated phases. The slight shift towards the longer wavelength can be attributed to the formal replacement of two O-donors by three more covalent N-donors in the crystal structure of non-hydrated europium(III) dicyanamide. Figure 9 shows the excitation and emission spectra of $Tb[N(CN)_2]_3 \cdot 2H_2O$ and $Tb[N(CN)_2]_3$. The excitation spectrum of $Tb[N(CN)_2]_3 \cdot 2H_2O$, monitored at $Tb^{3+}$ green emission at 545 nm ($^5D_4$-$^7F_5$), mainly consists of a broad band from 250 to 400 nm with a maximum at 300 nm and superimposed with sharp lines around 370 nm. The sharp lines originate from intra-4f transitions of $Tb^{3+}$. Excitation into the $4f^8$-$4f^75d$ transition of $Tb^{3+}$ at 300 nm yields the characteristic $^5D_4$-$^7F_J$ ($J$ = 3-6) emission of $Tb^{3+}$, with $^5D_4$-$^7F_5$ green emission as the most intense one ($\lambda_{max}$ = 545 nm). Similarly to $Eu[N(CN)_2]_3$, non-hydrated $Tb[N(CN)_2]_3$ shows a red shift (~10 nm) in the excitation maximum compared to hydrated $Tb[N(CN)_2]_3 \cdot 2H_2O$. This can be explained by the different local environment of $Tb^{3+}$ in the hydrated and non-hydrated compounds. The formation of two different crystal structures in turn affects the energy of the d orbital, resulting in excitation maxima at longer wavelengths. The CIE (Commission Internationale d'Eclairage) color coordinates (x, y) of $Ln[N(CN)_2]_3 \cdot 2H_2O$ and $Ln[N(CN)_2]_3$ with Ln = Eu, Tb are comparable to those of commercial red- and green-emitting phosphors (Table 2).[46,52]

The quantum efficiencies were measured for both hydrated and non-hydrated phases under monitoring wavelength of 365 nm to compare these phosphors with standard lamp phosphors. The QE study clearly shows that the hydrated phases exhibit comparatively lower efficiencies than the corresponding non-hydrated phases. It is well-known that the non-radiative effect of the OH oscillators of the $H_2O$ molecule affects the luminescence features of trivalent

lanthanides.[53] Therefore, comparatively low quantum efficiencies of hydrated dicyanamides can be explained with non-radiative losses by multiphonon emission involving the coordinated water molecules.

**Rare Earth Tricyanomelaminates**

Even more complex nitridocarbonates such as tricyanomelaminates ($[C_6N_9]^{3-}$) can by introduced into the coordination sphere of trivalent rare earth ions by ion exchange reactions. Tricyanomelaminates (TCM) can be regarded as the formal trimerization product of the dicyanamide ion. Depending on the pH value there are reports of non protonated, mono-protonated and diprotonated TCM complexes.[54-56] Starting from ammonium tricyanomelaminate and $LnCl_3{\cdot}xH_2O$ an isostructural series of nine lanthanide tricyanomelaminates, $[NH_4]Ln[HC_6N_9]_2[H_2O]_7{\cdot}H_2O$ (Ln = La, Ce, Pr, Nd, Sm, Eu, Gd, Tb, Dy) was obtained by ion exchange reactions.[57] The structure was found to be built up of $La^{3+}$ and two crystallographically independent monohydrogentricyanomelaminate ions $[HC_6N_9]^{2-}$, ammonium ions, and crystal water molecules (Figure 10). The monoprotonated $[HC_6N_9]^{2-}$ moieties in LaTCM form parallel layers perpendicular to [100] with an interlayer stacking distance of approximately 3.6 Å (Figure 11). The hydrogen atoms H1 and H10 are bound to the triazine ring nitrogen atoms N1 and N10, respectively. In the crystal structure of LaTCM, each $La^{3+}$ ion is surrounded by two nitrogen atoms from two different tricyanomelaminate moieties and seven oxygen atoms from crystal water molecules, forming nine-coordinated heptagonal-bi-pyramidal $LaN_2O_7$ polyhedra. The $[HC_6N_9]^{2-}$ ions are coordinated to $La^{3+}$ through their terminal nitrogen atoms N5 and N16. In the crystal structure of LaTCM, intermolecular hydrogen bonds are observed between the protonated ring atoms and the cyanamide side-arms of adjacent $[HC_6N_9]^{2-}$ moieties (N1-H1···N15 and N10-H10···N6), giving rise to an eight-membered ring-type arrangement, and thereby forming a tricyanomelaminate dimer (Figure 11). Because of the similarity of the X-ray powder patterns, the structures of the other eight rare earth tricyanomelaminates, LnTCM (Ln = Ce, Pr, Nd, Sm, Eu, Gd, Tb, Dy) were assumed to be isotypic and were refined by the Rietveld method, using the lattice parameters and the atomic coordinates of LaTCM as starting values.

The protonated TCM ligand has been assigned from the La compound by solid-state $^{1}H$, $^{13}C$, and $^{15}N\{^{1}H\}$ crosspolarization (CP) MAS NMR and advanced CP experiments such as crosspolarization combined with polarization inversion (CPPI) depicted in Figure 12. The $^{1}H$ 2D double-quantum single-quantum homonuclear correlation (DQ SQ) spectrum and the $^{15}N\{^{1}H\}$ 2D CP heteronuclear correlation (HETCOR) spectrum have revealed the hydrogen-

bonded (N-H···N) dimer of monoprotonated tricyanomelaminate moieties as well as H-bonding through $[NH_4]^+$ ions and $H_2O$ molecules.

Figure 13 shows the excitation and emission spectra of EuTCM. The excitation spectrum monitored at 615 nm shows a series of sharp lines between 300 and 550 nm attributable to $Eu^{3+}$ intra-4f transitions.[58] Unlike other $Eu^{3+}$ compounds, EuTCM does not show the typical Eu-N charge-transfer band in the excitation spectrum.[49] This indicates that the Eu-N charge-transfer band in EuTCM might be situated at much higher energy such that it cannot participate in the excitation process. The emission spectrum of EuTCM, recorded at $\lambda_{exc}$ = 397 nm, is composed of the typical $Eu^{3+}$ intra $^4f_6$ emission lines, which can be assigned to transitions between the first excited state ($^5D_0$) and the ground multiplets ($^7F_{1\text{-}4}$).[58] Furthermore, the $^5D_0$-$^7F_1$ line is known to originate from a magnetic dipole transition, while the $^5D_0$-$^7F_2$ line originates from an electric dipole transition.[59]

The excitation spectrum of TbTCM, monitored at the $Tb^{3+}$ green emission at 545 nm ($^5D_4$-$^7F_5$), mainly consists of a wide band between 240 and 400 nm with a maximum at 300 nm, superimposed with sharp lines at around 370 and 380 nm, and a further sharp line at 488 nm (Figure 14). The diffuse reflectance spectrum also shows a sharp absorption at 488 nm and a broad band at 300 nm. The sharp lines originate from intra-4f transitions of $Tb^{3+}$. The broad band can be assigned to the $^4f_8$-$^4f_7$5d transition of $Tb^{3+}$.[58] In fluoro and oxo compounds, the $^4f_8$-$^4f_7$5d transition of $Tb^{3+}$ is generally observed at higher energy. In the present case, a shift of the f–d transitions to lower energies can be expected due to the nephelauxetic effect. Excitation of the $^4f_8$-$^4f_7$5d transition of $Tb^{3+}$ at 300 nm yields the characteristic $^5D_4$-$^7F_J$ ($J$ = 3–6) emission of $Tb^{3+}$, with $^5D_4$-$^7F_5$ green emission as the most intense band ($\lambda_{max}$ = 545 nm). The CIE color coordinates (x, y) of EuTCM and TbTCM as well as quantum efficiencies are summarized in Table 2.

## Conclusion

During the six year funding period by the DFG Schwerpunktprogramm „Lanthanoidspezifische Funktionalitäten in Molekül und Material“ (SPP 1166, project SCHN 377/10), a variety of inventive synthetic strategies targeting new (oxo)nitridocarbonates was

elaborated. The reaction of $Cp_3Ln$ complexes with $NH_3$ and $CO_2$ was studied in detail and metalorganic intermediates like $[Cp_3LnNH_3]$, $[Cp_2LnNH_2]_2$ and carbamates were investigated by means of crystallographic and spectroscopic methods. The amine and amido complexes could be transferred into nanocrystalline LnN powders, whereas the carboxylation reactions with supercritical $CO_2$ yielded amorphous lanthanide carbamate compounds. These carbamate complexes could be utilized by means of pyrolysis reaction to obtain the hitherto unknown dioxy mono-carbodiimides of the smaller lanthanide ions (Y, Ho-Yb). With this novel synthetic approach we were able to synthesize phase-pure $Ln_2O_2CN_2$ starting from $NH_3$ and $CO_2$ by employing the well-known $Cp_3Ln$ complexes as molecular precursors. Utilizing urea as O/C/N donor for the synthesis of new oxonitridocarbonates led to the discovery of both urea complexes as well as homoleptic cyanates of $Sr^{2+}$ and $Eu^{2+}$. The reaction of Sr and Eu metal with urea at 130 °C and subsequent thermal treatment afforded the respective cyanates phase-pure and in nearly quantitative yields. The luminescence properties of all Eu containing compounds ($[Eu(OCN)_2(OC(NH_2)]$, $[Sr(OCN)_2(OC(NH_2)]:Eu^{2+}$, $Eu(OCN)_2$, $Sr(OCN)_2:Eu^{2+}$) were studied in detail from RT to 10 K. In addition to precursor and solid-sate approaches metathesis reaction via ion exchange in aqueous solutions were performed. Starting from lanthanide chlorides and sodium dicyanamide, hydrated $Ln[N(CN)_2]_3 \cdot 2H_2O$ as well as non-hydrated dicyanamides $Ln[N(CN)_2]_3$ of the lanthanides could be structurally characterized. Ion exchange reaction of lanthanide chlorides with ammonium tricyanomelaminate (TCM) afforded the series of nine isostructural lanthanide tricyanomelaminates $[NH_4]Ln[HC_6N_9]_2[H_2O]_7 \cdot H_2O$ (Ln = La, Ce, Pr, Nd, Sm, Eu, Gd, Tb, Dy). The $Eu^{3+}$ and the $Tb^{3+}$ compounds of both the dicyanamides as well as the tricyanomelaminates exhibit strong red/green luminescence, respectively. The luminescence was studied in detail comprising color coordinates, quantum yields, furthermore the electronic transitions have been assigned. The luminescence properties of all investigated compounds are still far from being suitable for industrial application, but as both oxidic and nitridic lanthanide doped host lattices play an important role for the development of new luminescence materials,[5] the comprehensive investigations in oxygen and nitrogen coordinating (oxo)nitridocarbonates might provide fundamental knowledge for the understanding of the correlation between luminescence properties and the crystallographic structure. In addition, the obtained compounds are promising precursors for the synthesis of new oxidic as well as nitridic materials, as some of them are easy to synthesize from line chemicals (e.g. urea).

**Acknowledgments**

Our investigations summarized in this review have been performed between 2004 and 2010 at the University of Munich (LMU). The work extensively has been supported by the Deutsche Forschungsgemeinschaft (DFG) within the Schwerpunktprogramm „Lanthanoidspezifische Funktionalitäten in Molekül und Material“ (SPP 1166, project SCHN 377/10). Furthermore we are indebted to the Fonds der Chemischen Industrie, Germany, for additional financial support. The authors acknowledge gratefully grants for Dr. S. Pagano and Dr. M. Zeuner by the Dr. Klaus Römer foundation, Munich. The authors would like to express their deep gratitude and acknowledgement to the chairmen Prof. R. Kempe, Bayreuth, and Prof. P. Roesky, Karlsruhe, for their superior style of initiation and guidance of this DFG-Schwerpunktprogramm, and we thank all participants of this program for valuable and fruitful discussions, many cooperations, and critical comments.

**Scheme 1.** Reaction pathways to lanthanide nitridic material and lanthanide dioxy monocarbodiimides starting from homoleptic cyclopentadienyl complexes. 1 Ln = Y, Sm, Gd, Dy, Ho, Er, Yb, Lu; 2 Ln = Sm, Gd, Dy, Ho, Er, Yb; 3 Ln = Dy, Ho, Er, Yb; 4 Ln = Sm, Gd, Dy, Ho, Er, Yb; 5 Ln = Er; 6 Ln = Y, Ho, Er, Yb, Lu; 7 Ln = Y, Ho, Er, Yb.

**Scheme 2.** Reaction of metals M = Sr, Eu with urea.

**Table 1.** Luminescence properties of $[Eu(OCN)_2(urea)]$, $[Sr(OCN)_2(urea)]:Eu^{2+}$, $Eu(OCN)_2$, $Sr(OCN)_2:Eu^{2+}$, and $Sr(SCN)_2:Eu^{2+}$.[45]

| | $[Eu(OCN)_2(urea)]$ | $[Sr(OCN)_2(urea)]:Eu^{2+}$ | $Eu(OCN)_2$ | $Sr(OCN)_2:Eu^{2+}$ | $Sr(SCN)_2:Eu^{2+}$[45] |
|---|---|---|---|---|---|
| $\lambda_{emmax}$ / nm[a] | 513 | 501 | 475 | 457 | 508 |
| $\nu_{emmax}$ / $cm^{-1}$[a] | 19480 | 19960 | 21040 | 21900 | 19685 |
| FWHM /$cm^{-1}$ (nm)[a] | 1935 (51) | 2180 (55) | 1870 (42) | 2115 (44) | 1550 (40) |
| $\lambda_{excmax}$ / nm[a] | 454 | 425 | 422 | 421 | 426 |
| $\nu_{excmax}$ / $cm^{-1}$[a] | 22000 | 23500 | 23700 | 23770 | 23474 |
| *Stokes Shift* /$cm^{-1}$ (nm)[a] | 3500 (59) | 4500 (76) | 2660 (53) | 1870 (36) | 3789 (82) |
| $T_{quench}$ / K | 140 | 170 | 140 | 160 | 220 |
| $T_{1/2}$ / K | 60 | 65 | 35 | 65 | 157 |

[a] at 10 K

**Table 2.** Luminescence properties of $Ln[N(CN)_2]_3 \cdot 2H_2O$, $Ln[N(CN)_2]_3$ and $[NH_4]Ln[HC_6N_9]_2[H_2O]_7 \cdot H_2O$ (Ln = Eu, Tb).

| phase | CIE color coordinates | | QE / % | reference |
|---|---|---|---|---|
| | x | y | ($\lambda_{exc}$ = 365 nm) | |
| $Eu[N(CN)_2]_3 \cdot 2H_2O$ | 0.633 | 0.359 | 6 | perylene dye (BASF) |
| $Eu[N(CN)_2]_3$ | 0.638 | 0.356 | 10.5 | perylene dye (BASF) |
| $Tb[N(CN)_2]_3 \cdot 2H_2O$ | 0.319 | 0.509 | 18 | $SrSi_2N_2O_2$:Eu (Philips) |
| $Tb[N(CN)_2]_3$ | 0.334 | 0.568 | 25.4 | $SrSi_2N_2O_2$:Eu (Philips) |
| $[NH_4]Eu[HC_6N_9]_2[H_2O]_7 \cdot H_2O$ | 0.618 | 0.362 | 6 | perylene dye (BASF) |
| $[NH_4]Tb[HC_6N_9]_2[H_2O]_7 \cdot H_2O$ | 0.325 | 0.575 | 18 | $SrSi_2N_2O_2$:Eu (Philips) |

**Figure 1**. a, b) SEM image of ErN showing the bulky nitride powder. c) TEM image of ErN crystallites. d) Corresponding ED pattern showing the ErN phase.[34]

**Figure 2**. Crystal structure of $Ln_2O_2CN_2$ (Ln = Ce - Gd; Ho, Er, Yb). Left along [001] and right along [010], Ln big gray, O small gray, C black, N white.

**Figure 3**. Left, view along the [100] direction of $[Eu(OCN)_2(urea)]$; right, view along the [010] direction. Eu-N/O polyhedra gray, O white, C black, N black/white, H atoms have been omitted for clarity. Ellipsoids at 50 % probability level.[40]

**Figure 4**. Left, representation of the $M(OCN)_8$ polyhedra; right, view of the $M(OCN)_2$ structure along [100], disregarding that every polyhedron is further connected to four neighboring polyhedra.[40]

**Figure 5**. The coordination sphere of $Ln^{3+}$ in $Ln[N(CN)_2]_3 \cdot 2\ H_2O$; Ln = Eu, Gd, Tb.[49]

**Figure 6**. Polyhedral representation of the structure of $Ln[N(CN)_2]_3 \cdot 2\ H_2O$ along [100]. Ln big white, C black, N gray, O small white and H small black spheres.[49]

**Figure 7**. Coordination sphere of $Ln^{3+}$ in $Ln[N(CN)_2]_3$ with Ln = La, Ce, Pr, Nd, Sm, Eu, Gd, Eu.

**Figure 8**. Excitation ($\lambda_{em}$ = 616 nm) and emission ($\lambda_{exc}$ = 365 nm) spectra of $Eu[N(CN)_2]_3 \cdot 2\ H_2O$ (solid line) and $Eu[N(CN)_2]_3$ (dotted line).[49]

**Figure 9**. Excitation ($\lambda_{em}$ = 545 nm) and emission ($\lambda_{exc}$ = 365 nm) spectra of $Tb[N(CN)_2]_3 \cdot 2\ H_2O$ (solid line) and $Tb[N(CN)_2]_3$ (dotted line).[49]

**Figure 10**. Representation of one formula unit of the unit cell of $[NH_4]La[HC_6N_9]_2[H_2O]_7 \cdot H_2O$. The hydrogen atoms of the $[NH_4]^+$ group and water molecules have been omitted.[57]

**Figure 11**. Views along the *a* axis (a), showing hydrogen bonding between two tricyanomelaminates, and along the *c* axis (b) of the unit cell of $[NH_4]La[HC_6N_9]_2[H_2O]_7 \cdot H_2O$, showing the parallel stacking of $[HC_6N_9]^{2-}$ moieties perpendicular to the *a* axis. The hydrogen atoms of the $[NH_4]^+$ group and water molecules have been omitted.[57]

**Figure 12**. $^{13}C$ and $^{15}N$ chemical shifts observed for $[NH_4]La[HC_6N_9]_2[H_2O]_7 \cdot H_2O$.[57]

**Figure 13**. The diffuse reflectance (REF), excitation (EXC), and emission (EM) spectra of $[NH_4]Eu[HC_6N_9]_2[H_2O]_7 \cdot H_2O$ at room temperature. The excitation and emission spectra were recorded at $\lambda_{em}$ = 615 nm and $\lambda_{exc}$ = 397 nm, respectively.[57]

**Figure 13**. The diffuse reflectance (REF), excitation (EXC), and emission (EM) spectra of $[NH_4]Tb[HC_6N_9]_2[H_2O]_7 \cdot H_2O$ at room temperature. The excitation and emission spectra were recorded at $\lambda_{em}$ = 545 nm and $\lambda_{exc}$ = 310 nm, respectively.

## References


[1] F. T. Edelmann, *Chem. Soc. Rev.* **2009**, *38*, 2253-2268.

[2] C. Meermann, K. W. Toernroos, W. Nerdal, R. Anwander, *Angew. Chem.* **2007**, *119*, 6628-6633; *Angew. Chem., Int. Ed.* **2007**, *46*, 6508-6513.

[3] N. S. Babu, R. Sree, P. S. S. Prasad, N. Lingaiah, *Energy Fuels* **2008**, *22*, 1965-1971.

[4] J. Fidler, D. Suess, T. Schrefl, *Handbook of Magnetism and Advanced Magnetic Materials* **2007**, *4*, 1945-1968.

[5] R-J. Xie, N. Hirosaki, *Sci. Technol. Adv. Mater.* **2007**, *8*, 588-600.

[6] Y. Hashimoto, M. Takahashi, S. Kikkawa, F. Kanamaru, *J. Solid State Chem.* **1995**, *114*, 592-594.

[7] Y. Hashimoto, M. Takahashi, S. Kikkawa, F. Kanamaru, *J. Solid State Chem.* **1996**, *125*, 37-42.

[8] E. Saeilynoja, M. Lastusaari, J. Hoelsaea, P. Porcher, *J. Lumin.* **1997**, *72*, 201-203.

[9] J. Holsa, R.-J. Lamminmaki, M. Lastusaari, P. Porcher, E. Sailynoja, *J. Alloys Compd.* **1998**, *275-277*, 402-406.

[10] J. Holsa, R.-J. Lamminmaki, M. Lastusaari, E. Sailynoja, P. Porcher, P. Deren, W. Strek, *Spectrochim. Acta, Part A:* **1998**, *54*, 2065-2069.

[11] M. Takahashi, Y. Hashimoto, S. Kikkawa, H. Kobayashi, *Zairyo* **2000**, *49*, 1230-1234.

[12] T. Takeda, N. Hatta, S. Kikkawa, *Chem. Lett.* **2006**, *35*, 988-989.

[13] M. Li, W. Yuan, J. Wang, C. Gu, H. Zhao, *Powder Diffr.* **2007**, *22*, 59-63.

[14] J. Sindlinger, J. Glaser, H. Bettentrup, T. Jüstel, H.-J. Meyer, *Z. Anorg. Allg. Chem.* **2007**, *633*, 1686-1690.

[15] M. Lei, H. Z. Zhao, H. Yang, B. Song, L. Z. Cao, P. G. Li, W. H. Tang, *J. Alloys Compd.* **2008**, *460*, 130-137.

[16] M. Zeuner, S. Pagano, W. Schnick, *Chem. Eur. J.* **2008**, *14*, 1524-1531.

[17] J. Glaser, H.-J. Meyer, *Angew. Chem.* **2008**, *120*, 7658-7661; *Angew. Chem., Int. Ed.* **2008**, *47*, 7547-7550.

[18] R. Srinivasan, S. Tragl, H. J. Meyer, *Z. Anorg. Allg. Chem.* **2005**, *631*, 719-722.

[19] J. Glaser, L. Unverfehrt, H. Bettentrup, G. Heymann, H. Huppertz, T. Juestel, H. J. Meyer, *Inorg. Chem.* **2008**, *47*, 10455-10460.

[20] L. Unverfehrt, M. Stroebele, J. Glaser, H. J. Meyer, *Z. Anorg. Allg. Chem.* **2009**, *635*, 1947-1952.

[21] W. Liao, C. Hu, R. K. Kremer, R. Dronskowski, *Inorg. Chem.* **2004**, *43*, 5884-5890.

[22] O. Reckeweg, F. J. DiSalvo, *Z. Anorg. Allg. Chem.* **2003**, *629*, 177-179.

[23] U. Baisch, S. Pagano, M. Zeuner, W. Schnick, *Eur. J. Inorg. Chem.* **2006**, 3517-3524.

[24] B. Juergens, E. Irran, W. Schnick, *J. Solid State Chem.* **2005**, *178*, 72-78.

[25] M. S. Wickleder, *Chem. Rev.* **2002**, *102*, 2011-2087.

[26] J. Liu, E. A. Meyers, J. A. Cowan, S. G. Shore, *Chem. Commun.* **1998**, *18*, 2043-2044.

[27] W. Schnick, R. Bettenhausen, B. Götze, H. A. Hoeppe, H. Huppertz, E. Irran, K. Koellisch, R. Lauterbach, M. Orth, S. Rannabauer, T. Schlieper, B. Schwarze, F. Wester, *Z. Anorg. Allg. Chem.* **2003**, *629*, 902-912.

[28] W. Schnick, *Angew. Chem.* **1999**, *111*, 3511 –3512; *Angew. Chem. Int. Ed.* **1999**, *38*, 3309 –3310.

[29] U. Baisch, S. Pagano, M. Zeuner, J. Schmedt auf der Günne, O. Oeckler, W. Schnick, *Organometallics* **2006**, *25*, 3027-3033.

[30] J. M. Birmingham, G. Wilkinson, *J. Am. Chem. Soc.* **1956**, *78*, 42-44.

[31] E. O. Fischer, H. Fischer, *J. Organomet. Chem.* **1966**, *6*, 141-148.

[32] R. D. Fischer, H. Fischer, *J. Organomet. Chem.* **1965**, *4*, 412-414.

[33] H. Fischer, *Doctoral thesis,* Technische Hochschule München, Germany, **1965**.

[34] U. Baisch, S. Pagano, M. Zeuner, N. Barros, L. Maron, W. Schnick, *Chem. Eur. J.* **2006**, *12*, 4785-4798.

[35] J. A. Behles, J. M. DeSimone, *Pure Appl. Chem.* **2001**, *73*, 1281-1285.

[36] P. Raveendran, Y. Ikushima, S. L. Wallen, *Acc. Chem. Res.* **2005**, *38*, 478-485.

[37] M. Solinas, J. Jiang, O. Stelzer, W. Leitner, *Angew. Chem.* **2005**, *117*, 2331-2335; *Angew. Chem. Int. Ed.* **2005**, *44*, 2291-2295.

[38] H. A. Baskin, U.S. Patent 19.620.711, **1963**.

[39] D. O. De Pree, K. L. Lindsay, U.S. Patent 2.801.154, **1957**.

[40] S. Pagano, G. Montana, C. Wickleder, W. Schnick, *Chem. Eur. J.* **2009**, *15*, 6186-6193.

[41] G. Meyer, *Z. Anorg. Allg. Chem.* **2008**, *634*, 201-222.

[42] W. Liao, R. Dronskowski, *Acta Crystallogr., Sect. E: Struct. Rep. Online* **2004**, *60*, i124.

[43] C. Wickleder, *Z. Anorg. Allg. Chem.* **2001**, *627*, 1693-1698.

[44] O. Reckeweg, A. Simon, *Z. Naturforsch., B: Chem. Sci.* **2003**, *58*, 1097-1104.

[45] C. Wickleder, *Chem. Mater.* **2005**, *17*, 1228-1233.

[46] R. Mueller-Mach, G. Mueller, M. R. Krames, H. A. Höppe, F. Stadler, W. Schnick, T. Juestel, P. Schmidt, *Phys. Status Solidi A* **2005**, *202*, 1727-1732.

[47] N. Yamashita, *J. Lumin.* **1994**, *59*, 195-199.

[48] A. -Q. Wu, F. -K. Zheng, W. -T. Chen, L. -Z. Cai, G. -C. Guo, J. -S. Huang, Z. -C. Dong, Y. Takano, *Inorg. Chem.* **2004**, *43*, 4839-4845.

[49] A. Nag, P. J. Schmidt, W. Schnick, *Chem. Mater.* **2006**, *18*, 5738-5745.

[50] A. Nag, W. Schnick, *Z. Anorg. Allg. Chem.* **2006**, *632*, 609-614.

[51] D. H. Dieke, *Spectra and Energy Levels of Rare-Earth Ions in Crystals*, Interscience Publishers; New York, 1968.

[52] M. Zeuner, F. Hintze, W. Schnick, *Chem. Mater.* **2009**, *21*, 336-342.

[53] R. M. Supkowski, W. D. Horrocks Jr., *Inorg. Chim. Acta* **2002**, *340*, 44-48.

[54] E. Irran, B. Juergens, W. Schnick, *Solid State Sci.* **2002**, *4*, 1305-1311.

[55] B. F. Abrahams, S. J. Egan, B. F. Hoskins, R. Robson, *Chem. Commun.* **1996**, 1099-1100.

[56] B. F. Abrahams, S. J. Egan, B. F. Hoskins, R. Robson, *Acta Crystallogr., Sect. C: Cryst. Struct. Commun.* **1996**, *52*, 2427-2429.

[57] A. Nag, B. V. Lotsch, J. Schmedt auf der Günne, O. Oeckler, P. J. Schmidt, W. Schnick, *Chem. Eur. J.* **2007**, *13*, 3512-3524.

[58] G. Blasse, B. C. Grabmeier, *Luminescent Materials*, Springer, Berlin, **1998**.

[59] C. Görller-Walrand, K. Binnemans, *Handbook on the Physics and Chemistry of Rare-Earths, Vol. 25*, (Eds. : K. A. Gschneider, Jr. , L. Eyring), North Holland, Amsterdam, **1998**, Chapter 167.

Equation_1
5x0mm (600 x 600 DPI)

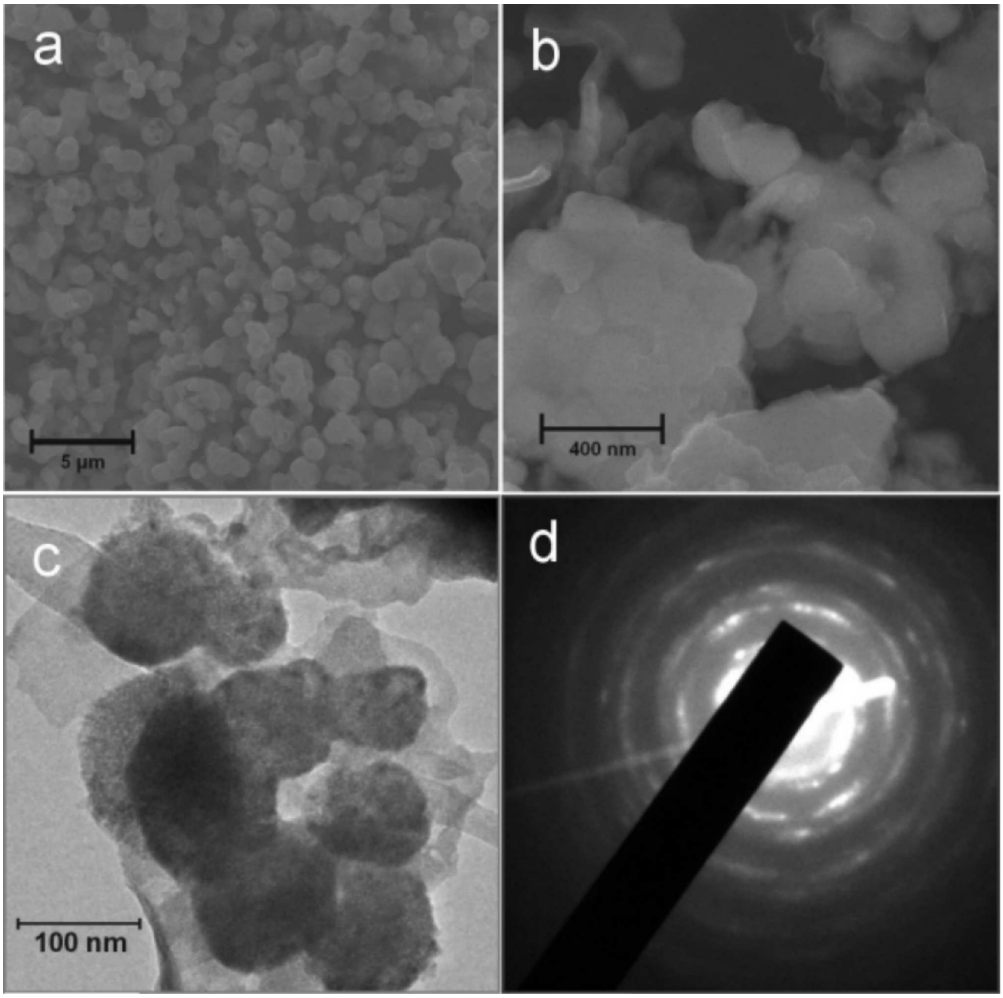


Figure_1
85x85mm (600 x 600 DPI)

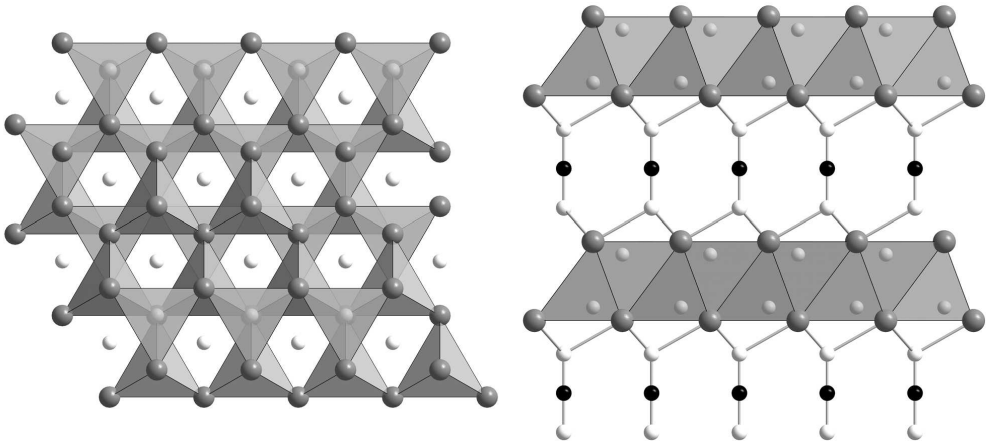

Figure_2
83x37mm (600 x 600 DPI)

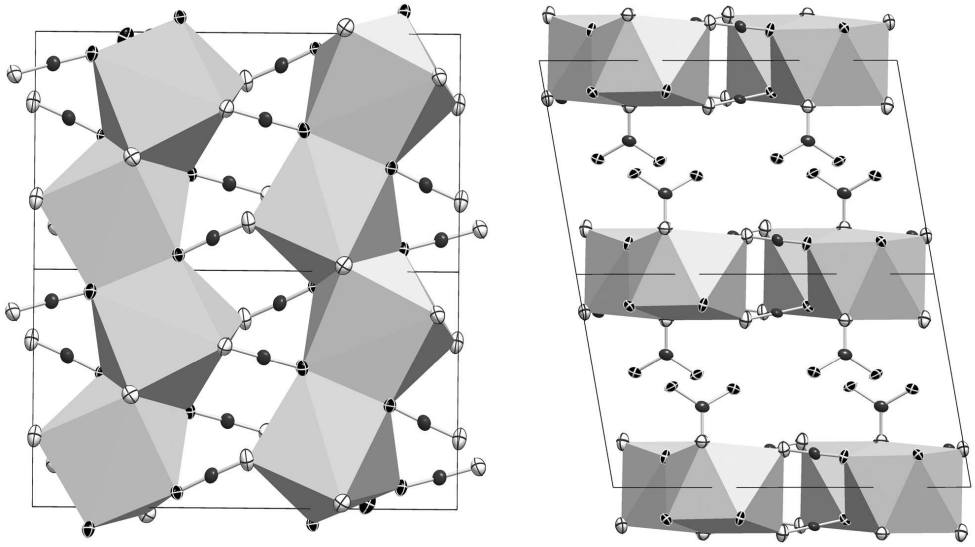

Figure_3
85x50mm (600 x 600 DPI)

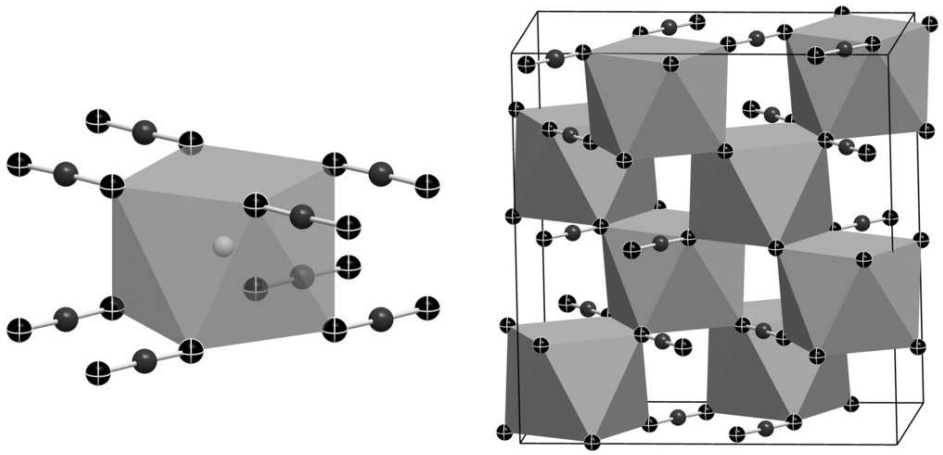

Figure_4
45x24mm (600 x 600 DPI)

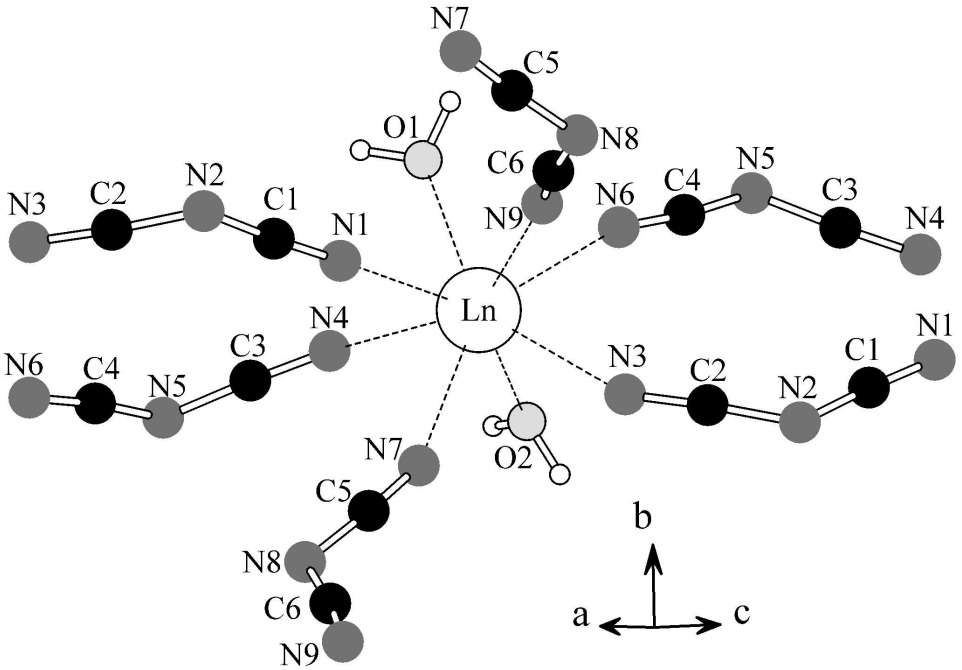
N7
C5
O1
N8
C6
N5
N2
C4
C3
N3
C2
C1
N1
N9
N6
N4
Ln
N4
C3
N1
N6
C4
N5
N3
C2
C1
N2
O2
N7
C5
b
N8
C6
a
c
N9

Figure_5

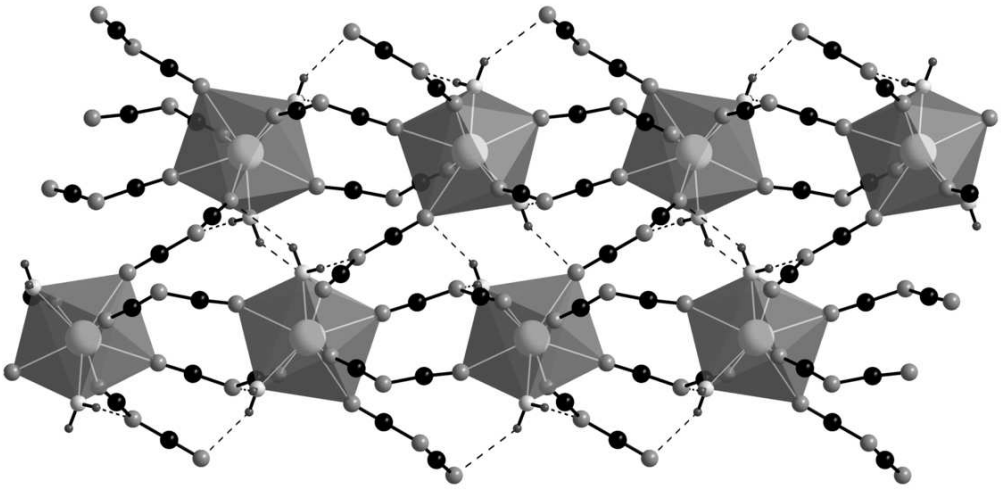

Figure_6
47x26mm (600 x 600 DPI)

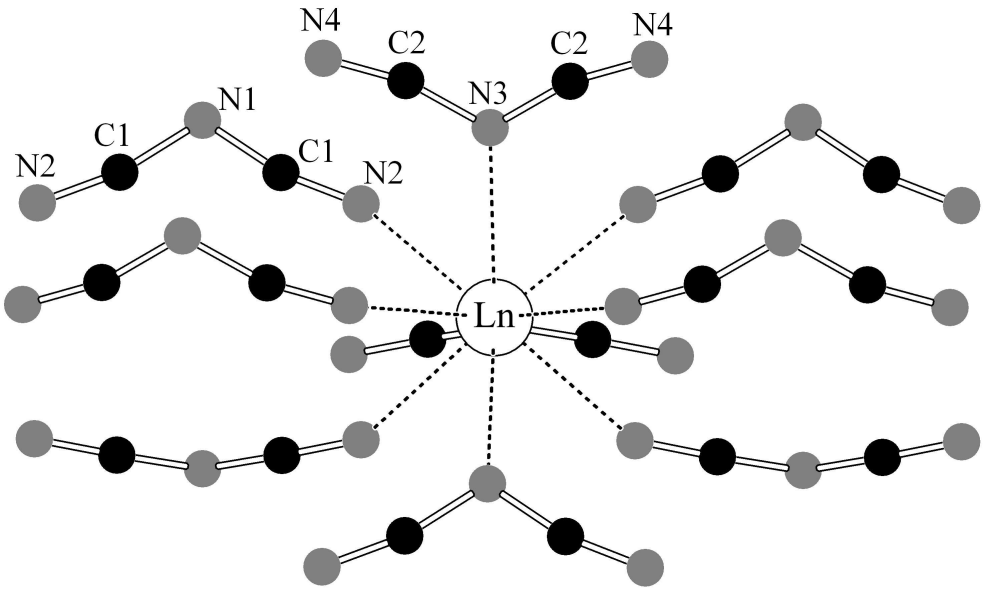


Figure_7

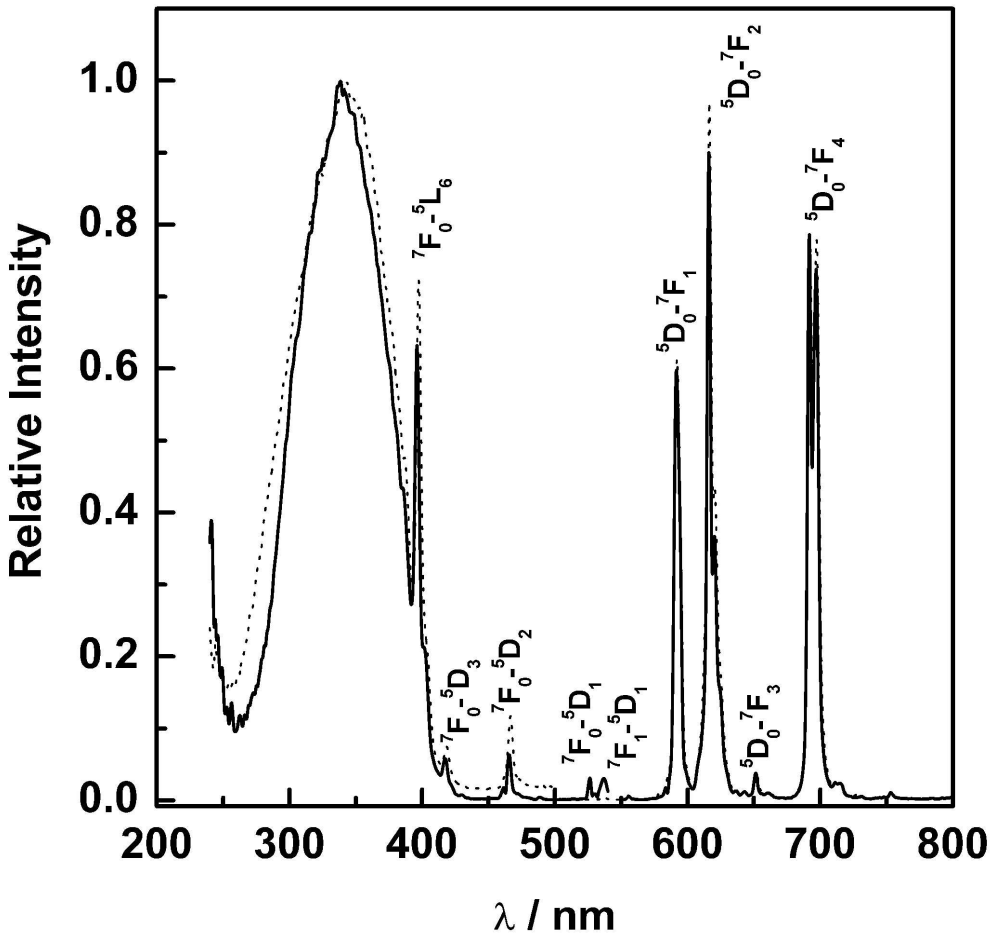


Figure_8
1466x1391mm (72 x 72 DPI)

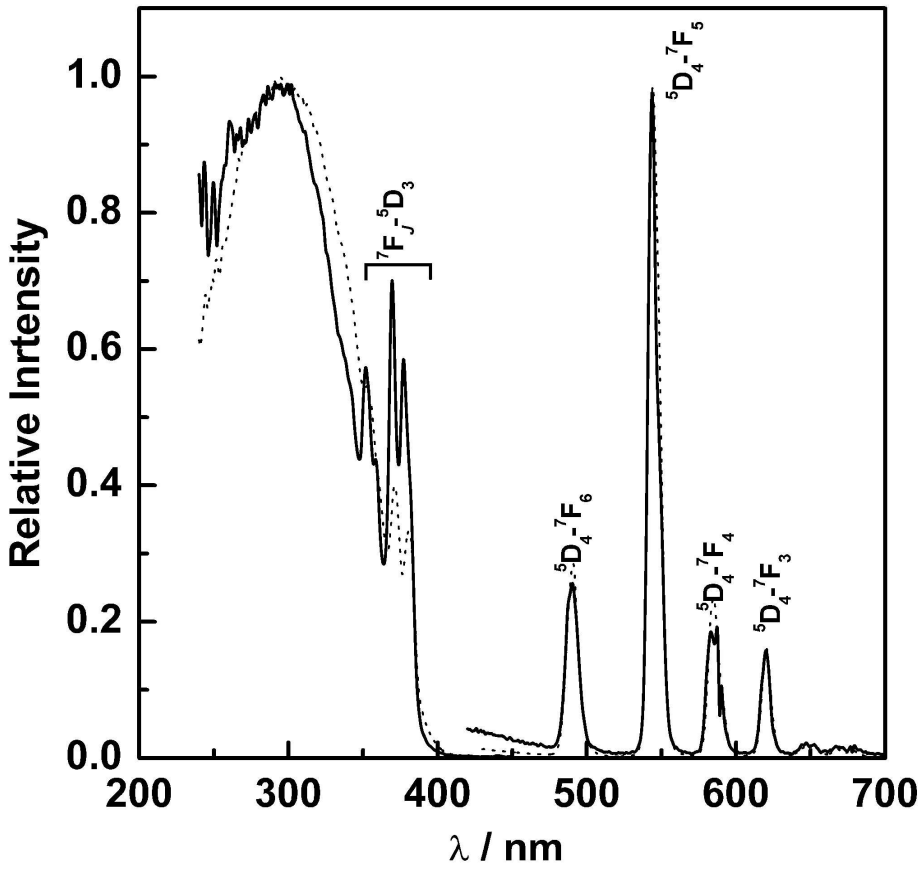


Figure_9
1174x1090mm (96 x 96 DPI)

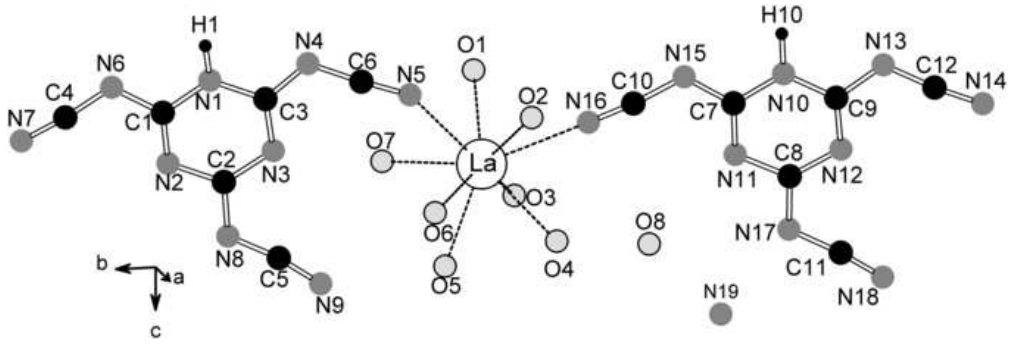


Figure_10
28x9mm (600 x 600 DPI)

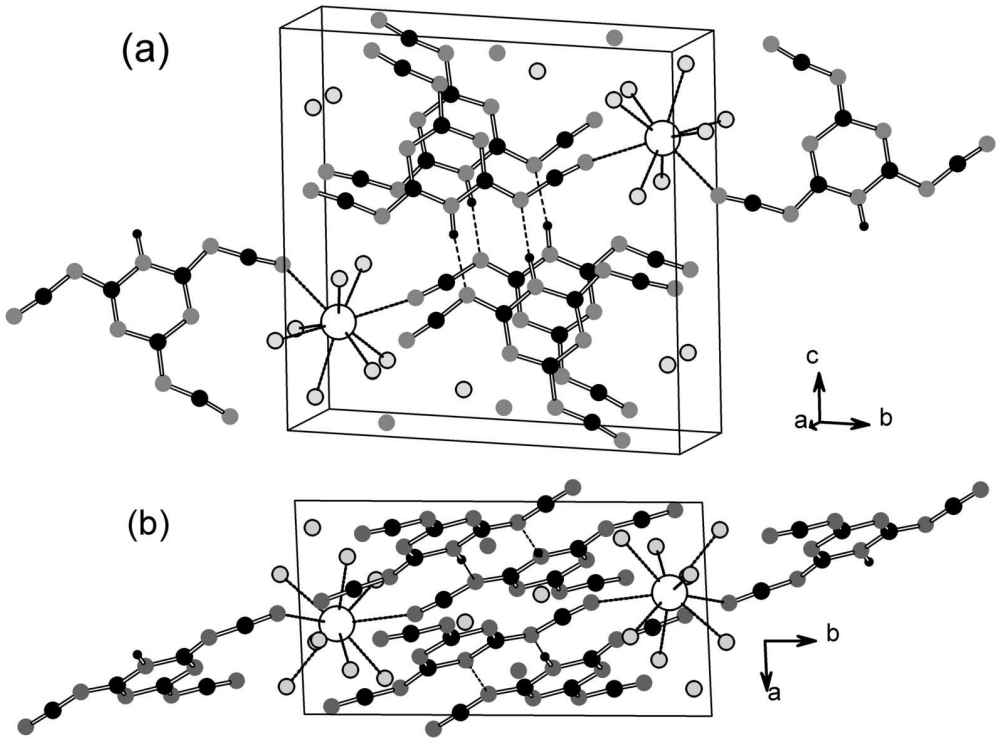


Figure_11
67x53mm (600 x 600 DPI)

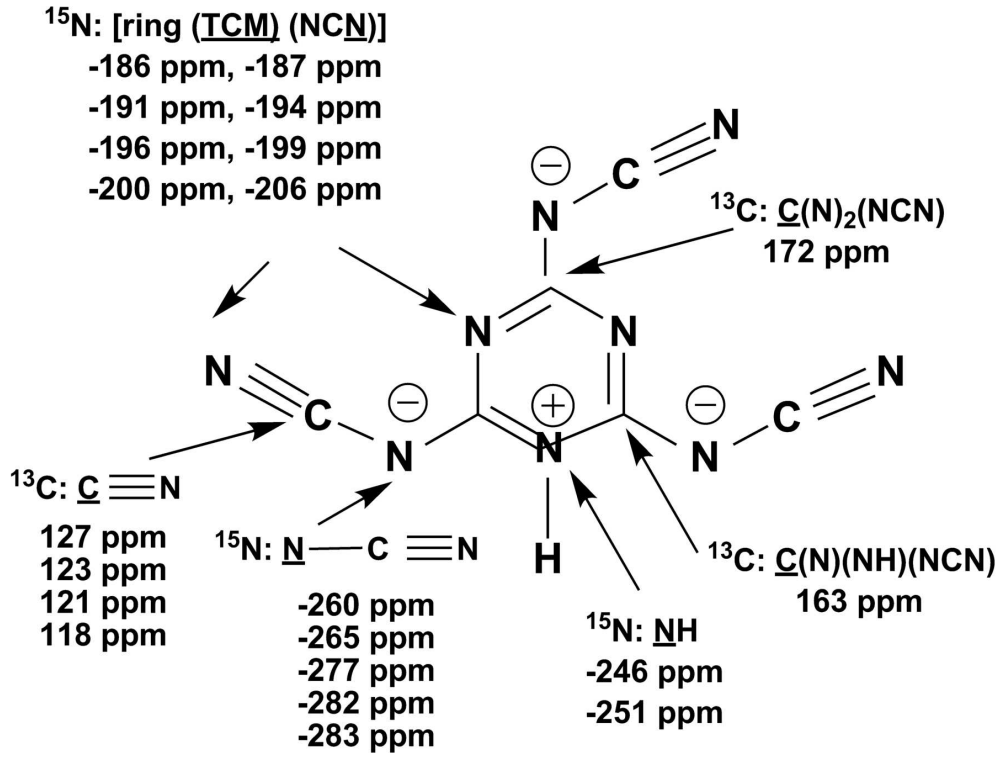


Figure_12
76x58mm (600 x 600 DPI)

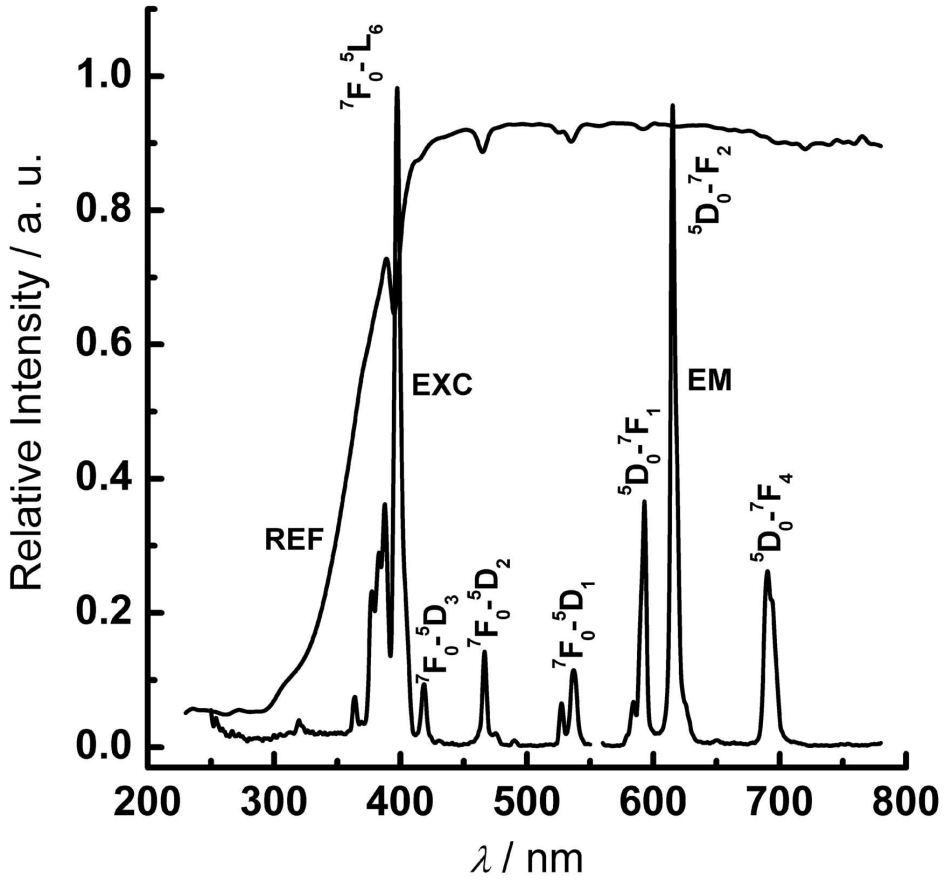


Figure_13
78x72mm (600 x 600 DPI)

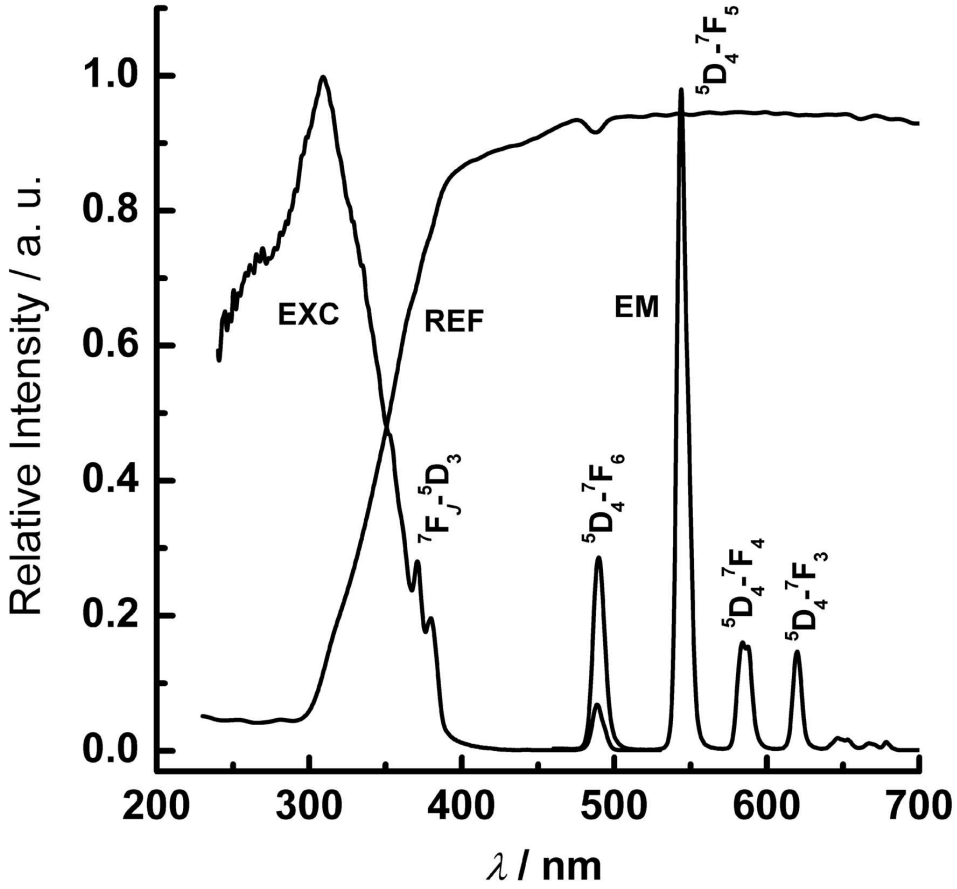


Figure_14
78x72mm (600 x 600 DPI)

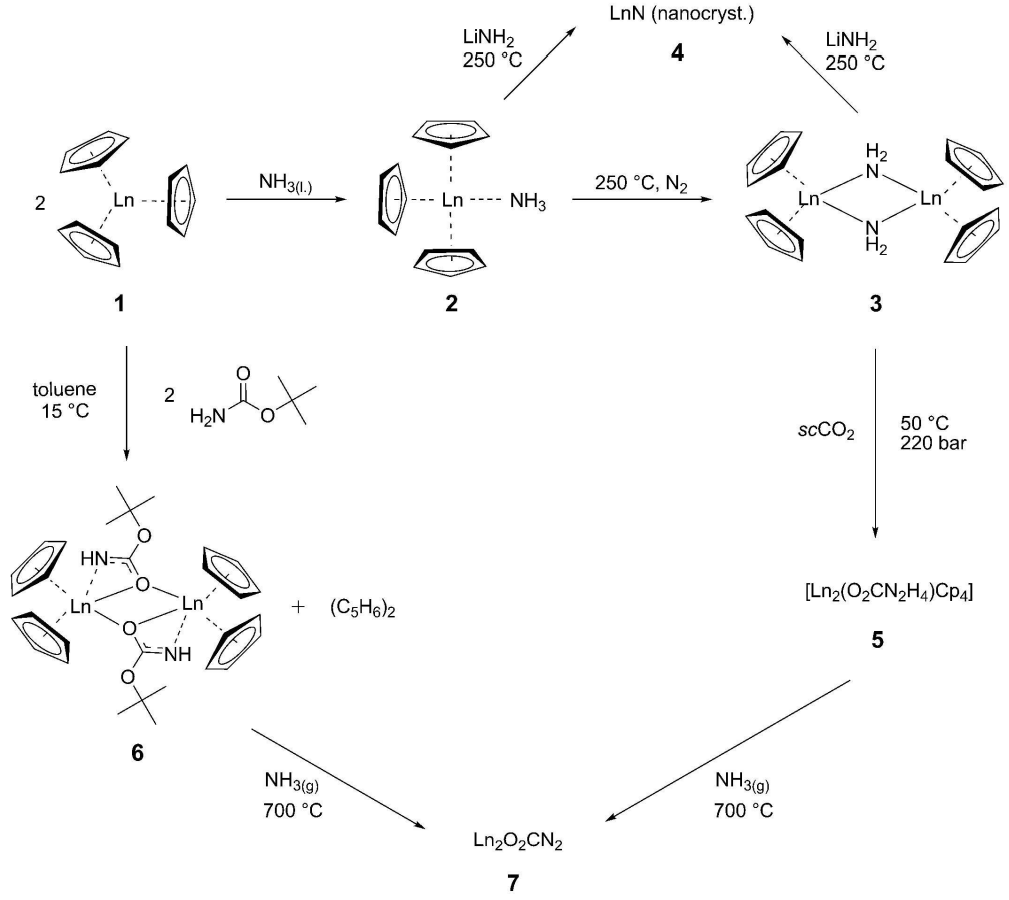


Scheme_1
180x162mm (600 x 600 DPI)

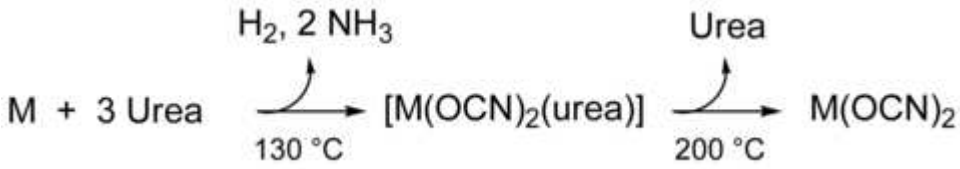


Scheme_2
20x3mm (600 x 600 DPI)